JOURNAL OF SOLID STATE CHEMISTRY 83, 188–197 (1989)

The Structure of the 44 K Superconductor $(Y_{1-x}Ca_x)Ba_2Cu_3O_{6+\delta}$ ($\delta \leq 0.2$)

JOHN B. PARISE[1] AND EUGENE M. McCARRON III

Central Research and Development Department, E. I. Du Pont de Nemours & Company, Experimental Station, P. O. Box 80356, Wilmington, Delaware 19880-0356

Received June 2, 1989; accepted August 7, 1989

Replacing Y(III) by Ca(II) in $(Y_{1-x}Ca_x)Ba_2Cu_3O_6$ induces superconductivity. A solid-solution limit exists, as is evidenced by the lack of variation in unit cell parameters for values of $x > 0.3$. At low nominal doping levels ($x < 0.3$), materials prepared by solid-state techniques consist of a complex intergrowth of Ca-rich and Ca-poor 123-type phases, as well as $YBa_2Cu_3O_6$ and $BaCuO_2$. At higher nominal doping levels the Ca content of the 123-type phase becomes constant ($x \sim 0.30$). Structural refinements using data collected by X-ray and neutron powder diffractometry are consistent with Ca-doping causing oxidation only of Cu in the sheet, leaving the copper in the so-called chain site as Cu(I). Many of the structural changes occurring in this system upon oxidation, such as a flattening of the CuO_2 sheets, a contraction of the in-plane Cu–O distance, and a decrease in the Cu–Cu distance between planes, also occur in the structurally related superconducting system, $Pb_2Sr_2(Y_{1-x}Ca_x)Cu_3O_8$.

Introduction

Recently we reported (*1*) on the observation of superconductivity in the absence of "chain oxygens" in $YBa_2Cu_3O_{6+\delta}$ ($\delta = 0$). This was achieved by the substitution of Ca(II) for Y(III) to produce compounds $(Y_{1-x}Ca_x)Ba_2Cu_3O_{6+\delta}$ which are tetragonal (*2, 3*) and still contain, for the most part, linearly coordinated Cu(I) in the chain site (Fig. 1). Furthermore, X-ray absorption measurements (*2, 3*) have confirmed that the amount of Cu(I) does not change as a function of x. These results imply that replacing Ca for Y oxidizes the CuO sheets (Fig. 1) and induces superconductivity in an analogous fashion to the metal doping experiments in La_2CuO_4 (*4–6*). By way of contrast, several investigators have similarly Ca-doped $YBa_2Cu_3O_7$ and reported a depression of the superconducting properties (*7*).

With regard to structure–property relationships, the deconvolution of structural changes, which occurs upon oxidation of the $YBa_2Cu_3O_{6+\delta}$ structure type, is made difficult if the doping mechanism is via oxygen insertion (*8, 9*). In this case, atomic displacements within the structure are a complex function of oxygen content, oxygen order, and electron counts on both the

[1] To whom all correspondence should be addressed at: Department of Earth and Space Sciences, State University of New York at Stony Brook, Stony Brook, NY 11794-2100.

0022-4596/89 $3.00

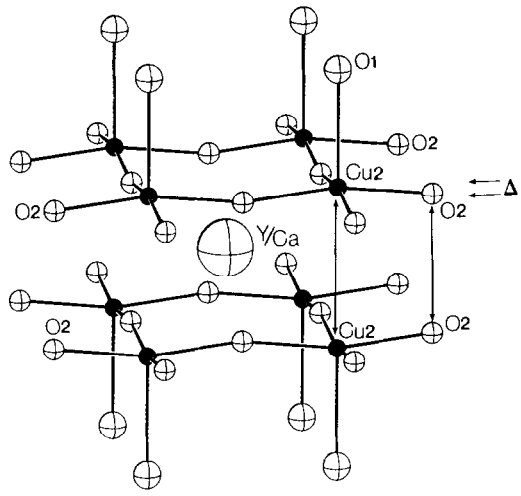

FIG. 1. The structure of $(Y_{1-x}Ca_x)Ba_2Cu_3O_6$ (*1*). Spheres, arbitrary in size, represent metal and oxygen atoms in the double sheet of CuO. Δ (see text and Table II) is a measure of the flatness of the sheet. The Cu(2)–Cu(2) and O(2)–O(2) distances, referred to in Table III, are indicated by double-headed arrows.

sheet and the chain structural elements (Fig. 1). On the other hand, the system $(Y_{1-x}Ca_x)Ba_2Cu_3O_6$ affords, in principle, an opportunity to study geometric changes commensurate with increasing levels of oxidation of the sheet without the complications arising from variable oxygen content.

In the structurally related system, $Pb_2Sr_2(Y_{1-x}Ca_x)Cu_3O_8$ (*3, 10–12*), oxidation of the sheets is once more due to Ca(II) replacing Y(III). However, the two systems have quite different values of T_c, with the value reported for the Sr-containing material some 10–15 K higher (*10, 11*). A comparison of the structural changes in these two materials as a function of Ca content—especially at the same Ca content—would be useful in estimating the relative importance of the formal oxidation state and structure in determining T_c.

Experimental

Samples were prepared in a manner outlined in recent papers (*1–3*). Nominal compositions were $(Y_{1-x}Ca_x)Ba_2Cu_3O_{6+\delta}$ [(Y,Ca)123-O_6], where $x = 0.10$, 0.25, 0.40, and 0.50. The value of δ has been determined from structural refinements based on neutron diffraction data (Table I) and does not exceed a value of 0.2 for any sample.

Results obtained using electron microscopy (*3*) have indicated that, for samples with $x \leq 0.3$, significant quantities of $YBa_2Cu_3O_{6+\delta}$ occur as an impurity phase (Table I). Further, for all values of x studied, $BaCuO_2$ was present (Table I). Because

TABLE I

EXPERIMENTAL DETAILS FOR ROOM TEMPERATURE DATA COLLECTED ON $(Y_{1-x}Ca_x)Ba_2Cu_2O_{6+\delta}$

Nominal x	0.10	0.25	0.40	0.50
Phases present[a]	Y,Y/Ca,B	Y,Y/Ca,B,*X*	Y,Y/Ca,B,*X*	Y/Ca,B,*X*
% B[b]	0.10	0.22	0.42	1.00
% Y[b]	30	23	10	0
Radiation	X-ray + neutron	Neutron	Neutron	Neutron
λ[c] (Å)	1.540 2.374	2.374	1.357	1,357
Monochromator (N)	Pyrolytic graphite (002)	Pyrolytic graphite (002)	Si(111)	Si(111)
Analyzer (N)	Pyrolytic graphite (004)	Pyrolytic graphite (004)	Pyrolytic graphite (004)	Pyrolytic graphite (004)
Collimation (N)	20′–40′–40′–20′	20′–40′–40′–20′	20′–40′–40′–20′	20′–40′–40′–20′
Phases refined[a,d]	Y,Y/Ca	Y/Ca	Y/Ca	Y/Ca

[a] Y = $YBa_2Cu_3O_{6+\delta}$, Y/Ca = $(Y_{1-x}Ca_x)Ba_2Cu_3O_{6+\delta}$; B = $BaCuO_2$; *X* = unknown, probably a Ca-rich phase.

[b] Mole% from ratio of refined scale factors based on neutron diffraction data.

[c] Wavelength (λ) fixed for X-ray data, refined for neutron (N) data with $x = 0.1$ and determined using CeO_2 standard (a = 5.4113 Å) for other neutron data.

[d] Atomic parameter refinement. Lattice parameters and scale factor for all phases, excepting *X*, refined for each data set. Atomic parameters for Y taken from refinement of sample with nominal $x = 0.10$. These parameters fixed for structure model of Y in more Ca-rich samples.

of the close correspondence of the cell parameters of Ca-containing and Ca-free 123-O_6 phases (Table II), the microanalytical results (*3*) have provided the chemical constraints required to analyze the results from neutron powder diffraction data. In particular, the analytical results confirm that Ca substitutes exclusively for Y since the Ba/Cu ratio is close to 0.67 for all samples (*3*) and, although the Y/Ca ratio varies at low values of x, (Y + Ca)/Cu is close to 0.33. In the refinements described below, Ba, Cu, and O sites (excepting the site at (0, $\frac{1}{2}$, 0), see Table II) are fixed at full occupancy. Consistent with the results of the microanalytical study (*3*), the Y site is presumed to be fully occupied by a mixture of Y and Ca only. The Y/Ca ratio varies somewhat within each sample; for a sample of nominal $x = 0.15$, individual analyses (*3*) varied from $x = 0.12$ to 0.17. Although the powder diffraction data does not allow us to distinguish between such a fine variation in Ca content, it does allow for the refinement of an average structure for the Ca-containing phase in a particular sample.

Neutron powder diffraction measurements were performed on a triple-axis dif-

TABLE II

REFINED PARAMETERS[a] FOR $(Y_{1-x}Ca_x)Ba_2CuO_{6+\delta}$

Nominal	x	0.0	0.1	0.25	0.4	0.5
Refined	x[b]		0.15(3)	0.24(4)	0.26(7)	0.28(6)
Refined	δ[c]	0.16(2)	0.16(2)	0.18(2)	0.20(2)	0.20(2)
	a (Å)	3.866(1)	3.862(1)	3.855(2)	3.854(2)	3.856(1)
	c (Å)	11.777(4)	11.844(4)	11.836(1)	11.809(1)	11.809(1)
$Y_{1-x}Ca_x$[d]	$U \times 10^2$	2.6(2)	−0.2(2)	0.5(2)	0.5(3)	0.7(2)
Ba[e]	z	0.1912(9)	0.1961(2)	0.1945(3)	0.1933(7)	0.1942(5)
	$U \times 10^2$	2.6(2)	0.7(1)	1.3(2)	0.9(2)	0.7(2)
Cu(1)[f]	$U \times 10^2$	2.6(2)	1.7(2)	1.6(2)	1.5(3)	2.0(2)
Cu(2)[g]	z	0.3597(8)	0.3560(3)	0.3603(2)	0.3614(5)	0.3617(5)
	$U \times 10^2$	2.6(2)	0.2(1)	0.7(2)	0.2(2)	0.8(2)
O(1)[g]	z	0.1521(8)	0.1524(4)	0.1519(4)	0.1521(8)	0.1523(7)
	$U \times 10^2$	2.6(2)	2.1(1)	2.5(2)	1.8(2)	2.8(2)
O(2)[h]	z	0.3778(6)	0.3777(2)	0.3775(2)	0.3753(5)	0.3758(4)
	$U \times 10^2$	2.6(2)	0.3(1)	0.8(1)	0.9(2)	1.2(1)
(R_{wp})[i]		0.11(0.07)		0.08	0.14	0.12
(S_p^2)[j]		1.86		3.01	3.20	6.0
(R_I)[j]		0.05		0.02	0.04	0.04

[a] Space group *P4/mmm* (No. 123).

[b] For 123-O_6 phase ($x = 0$), parameters taken from joint refinement using neutron and X-ray data of sample with nominal $x = 0.1$; thermal parameters (Å^2) constrained to be equal during refinement of this phase.

[c] Located at (0, $\frac{1}{2}$, 0); isotropic U constrained to 0.01 Å^2 for this site; value of δ assumed the same $YBa_2Cu_3O_{6+\delta}$ and $(Y_{1-x}Ca_x)Ba_2Cu_3O_{6+\delta}$ in the same sample.

[d] Position 1*d* (4/*mmm*) at ($\frac{1}{2}$, $\frac{1}{2}$, $\frac{1}{2}$).

[e] Position 2*h* (4/*mmm*) at ($\frac{1}{2}$, $\frac{1}{2}$, z).

[f] Position 1*a* (4/*mmm*) at (0, 0, 0).

[g] Position 2*g* (4*mm*) at (0, 0, z).

[h] Position 4*l* (2*mm*) at (0, $\frac{1}{2}$, z).

[i] Defintions for these discrepancy indexes given in Ref. (*13*). Number in parentheses is for X-ray powder data.

[j] Combined index based on all phases in the patterns used. Structures of phases with $x = 0$, 0.15(3) are refined jointly (see note (b) above).

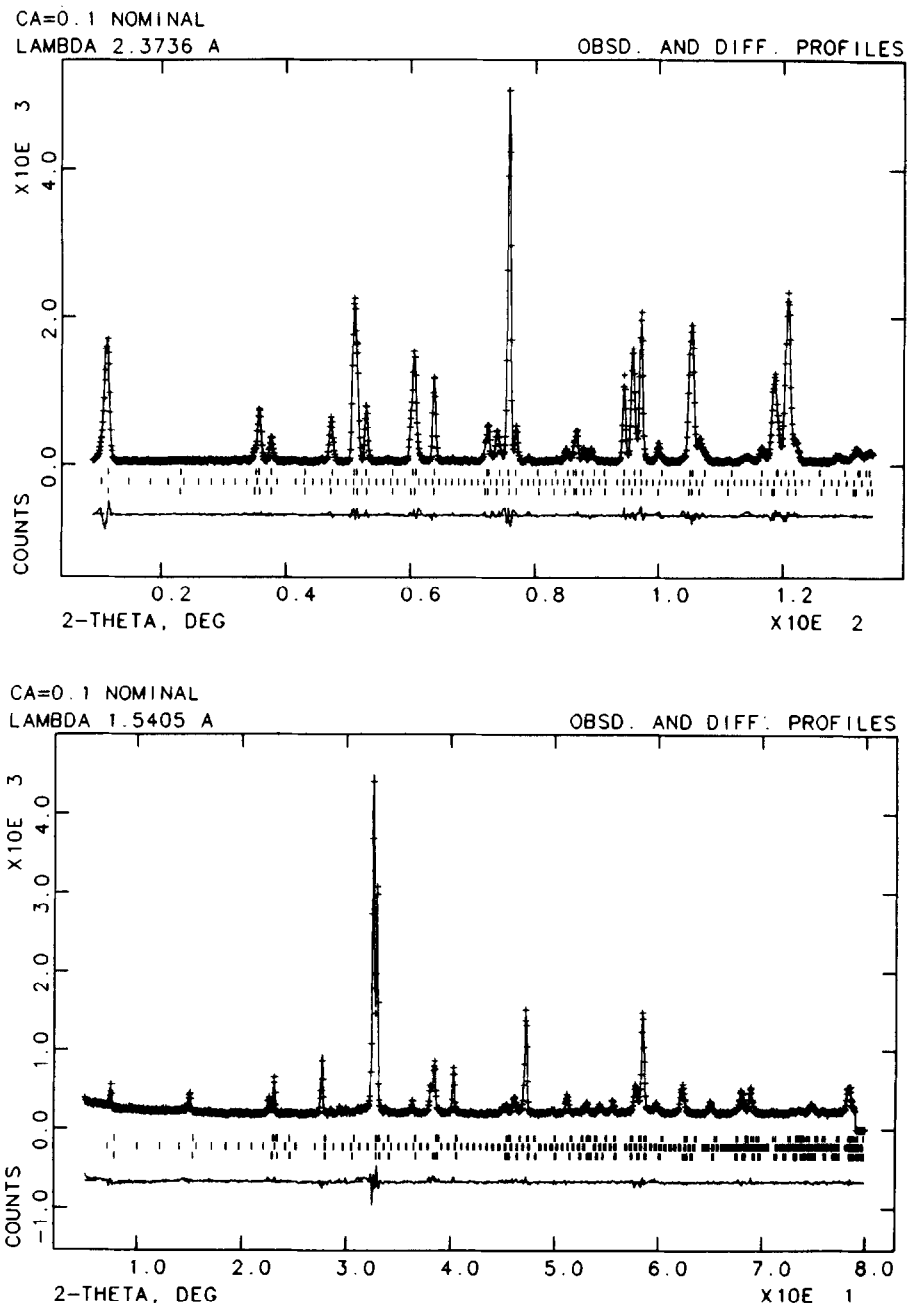

FIG. 2. Observed (crosses) and calculated (solid line) neutron (top) and X-ray (bottom) diffraction patterns for $(Y_{1-x}Ca_x)Ba_2Cu_3O_{6+\delta}$ ($x = 0.1$, nominal). Short vertical markers below the pattern represent allowed reflections for $YBa_2Cu_3O_{6+\delta}$ (top), $BaCuO_2$ (middle), and $(Y_{1-x}Ca_x)Ba_2Cu_3O_{6+\delta}$ (bottom).

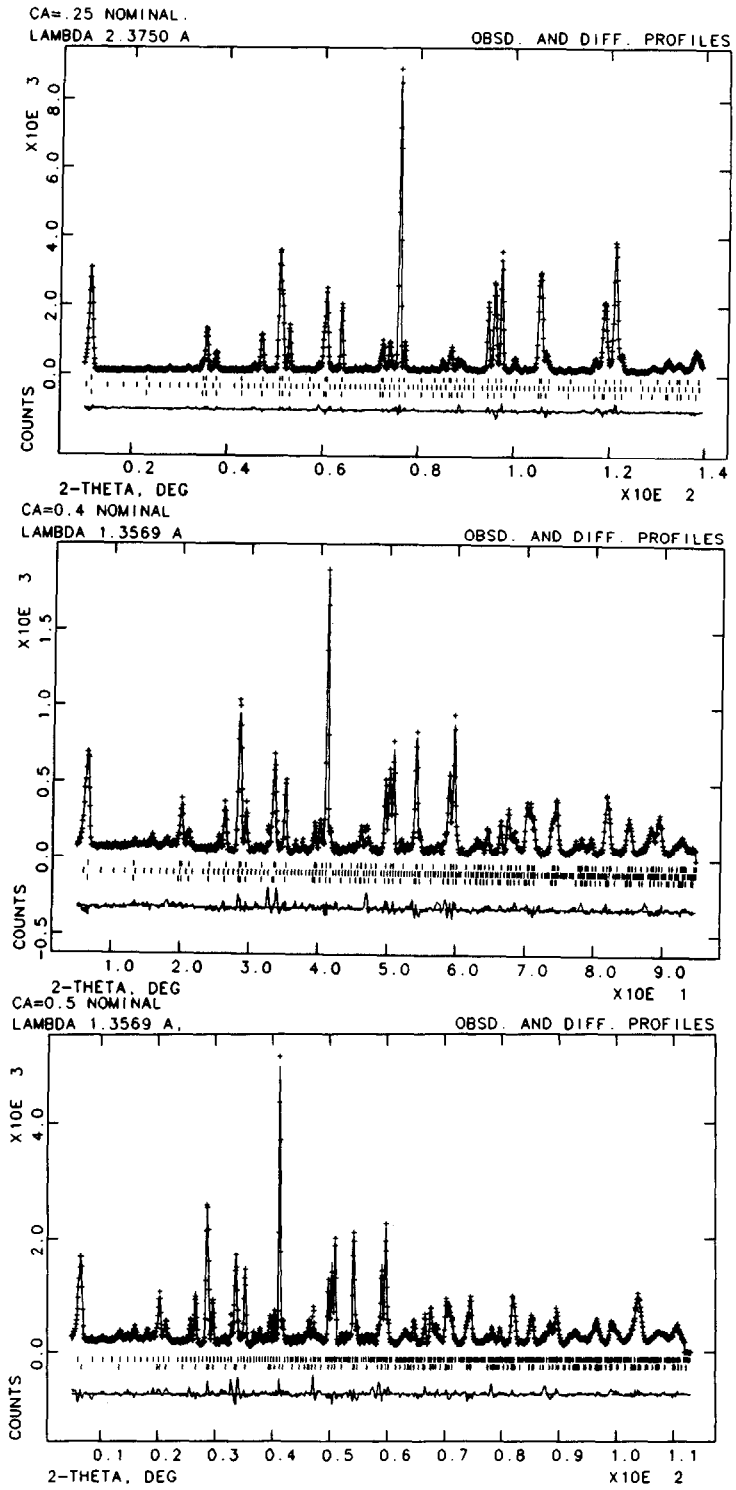

FIG. 3. Observed and calculated neutron powder diffraction patterns for nominal $x = 0.25, 0.40, 0.50$ (see Fig. 2 and Tables I and II). For the sample with nominal $x = 0.5$, only the calcium-containing phase and $BaCuO_2$ are considered.

TABLE III

SELECTED INTERATOMIC DISTANCES (Å) AND ANGLES (°) FOR $(Y_{1-x}Ca_x)Ba_2CuO_6$

Normal x	0.0	0.10	0.25	0.40	0.50
Refined x		0.15(3)	0.24(4)	0.26(7)	0.28(6)
Cu(1)–O(1)	1.792(15)	1.804(5)	1.797(5)	1.797(9)	1.798(9)
Cu(2)–O(1)	2.444(14)	2.458(5)	2.466(6)	2.472(8)	2.473(8)
Cu(2)–O(2)	1.945(2)	1.942(1)	1.938(1)	1.934(1)	1.935(1)
Cu(2)–Cu(2)	3.305(15)	3.316(5)	3.307(6)	3.272(8)	3.266(8)
O(2)–O(2)	2.880(15)	2.897(5)	2.900(6)	2.946(9)	2.933(9)
Y/Ca–Cu(2)	3.194(5)	3.195(2)	3.189(2)	3.179(4)	3.178(3)
Cu(2)–O(2)–Cu(2)	167.2(7)	167.6(2)	167.9(2)	170.3(6)	170.1(5)
$\Delta z \times 10^{2a}$	0.233	0.213	0.201	0.165	0.165

[a] The difference (Δ), in Å, between the plane (001) occupied by Cu(2) and O(2); Δ would be 0.000 if the Cu(2)–O(2) sheet were flat (Fig. 1).

fractometer at the H4S station of the Brookhaven high flux beam reactor. The instrument configuration and experimental conditions for each data set are summarized in Table I. For the neutron data, the higher order harmonics were eliminated with a pyrolytic graphite filter. The samples were all in the form of free-standing cylindrical pellets (20 g, 1.3 cm diameter, and 3 cm high).

Structure refinement was initiated using previously published coordinates (*1–3*) and the GSAS-Suite of programs (*14*), which allow for the simultaneous refinement of the structures of muliple phases contributing to X-ray and/or neutron diffraction patterns. For a sample of nominal composition $(Y_{0.9}Ca_{0.1})Ba_2Cu_3O_6$ (Table I), an X-ray data set (Cu$K\alpha$ radiation, Figs. 2 and 3) was also collected and combined with the neutron data in a simultaneous refinement of the structures of $(Y_{1-x}Ca_x)Ba_2Cu_3O_{6+\delta}$ and $YBa_2Cu_3O_{6+\delta}$. The atomic parameters of $BaCuO_2$ were not refined; those for $YBa_2Cu_3O_{6+\delta}$ were refined only in the sample having nominal $x = 0.1$ and subsequently constrained at these values for the remaining samples (Table I). The oxygen content (Table II) for Y/Ca and Y phases in the same sample was constrained to be equal during refinement (Table I). The validity of this constraint was tested in the sample

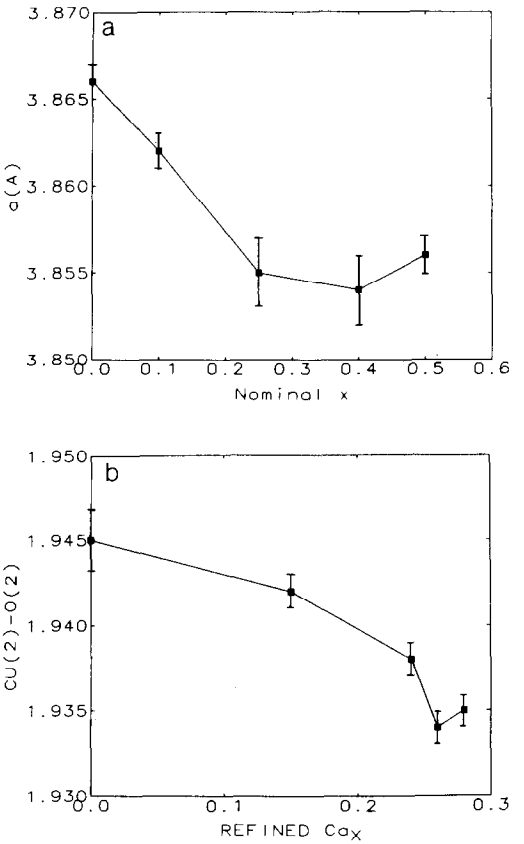

FIG. 4. (a) Variation of a unit cell parameter with nominal x and (b) of Cu(2)–O(2) distance (with a single sheet in Fig. 1) with refined x in the series $(Y_{1-x}Ca_x)Ba_2Cu_3O_{6+\delta}$ ($\delta \leq 0.20$).

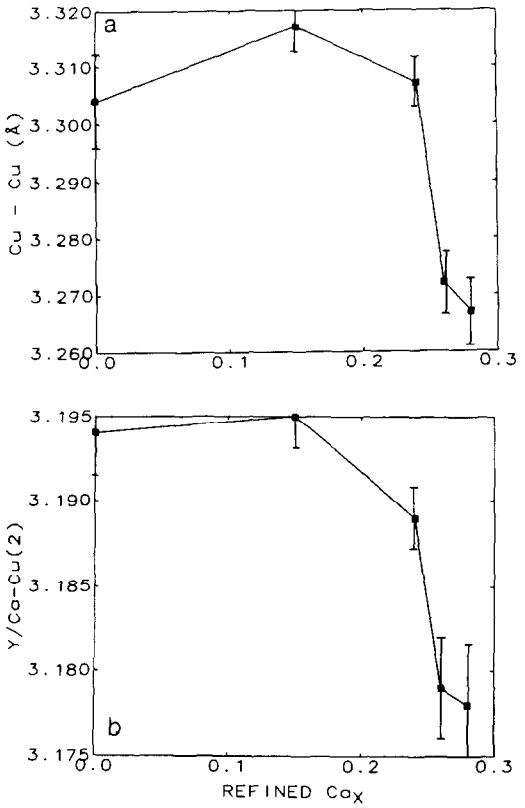

FIG. 5. Variation of (a) Cu(2)–Cu(2) distance (between the sheets as indicated in Fig. 2) and (b) Y/Ca–Cu(2) distance (Fig. 2) with the refined value of x in the series $(Y_{1-x}Ca_x)Ba_2Cu_3O_{6+\delta}$.

with nominal $x = 0.1$ (since it contains the largest proportion of $YBa_2Cu_3O_{6+\delta}$, Table I); the refined values of δ were 0.15(3) and 0.18(3), for Y/Ca and Y phases, respectively. Further, the occupancy of the site occupied by the oxygen atom coordinated to both Cu(1) and Cu(2) was varied (Fig. 1, Table II) and in all cases was found to be fully occupied within one estimated standard deviation (0.02).

The final refined models for Y/Ca and Y phases assumed fully occupied Y/Ca, Ba, Cu, O(1), and O(2) sites (Fig. 1). They are presented in Table I while selected bond lengths and angles derived from these models are given in Table III and in Figs. 4–6. The peak shape function (*13*), and its dependence on 2θ, were presumed to be the same for all phases in the same sample. When refinements were performed on samples with nominal values of $x < 0.3$ using only two phases, $Y_{1-x}Ca_xBa_2Cu_3O_6$ and $BaCuO_2$, inferior fits to the observed data were obtained. This is to be expected since electron microscopy (*3*) indicates that $YBa_2Cu_3O_{6+\delta}$ is also present in these samples.

Results

Changes in the structure of Y123-O_6 upon doping with Ca are of three types: those changing smoothly and monotonically [i.e., cell parameters, Cu(2)–O(2) and Cu(2)–O(1)]; those not changing [e.g., Cu(1)–

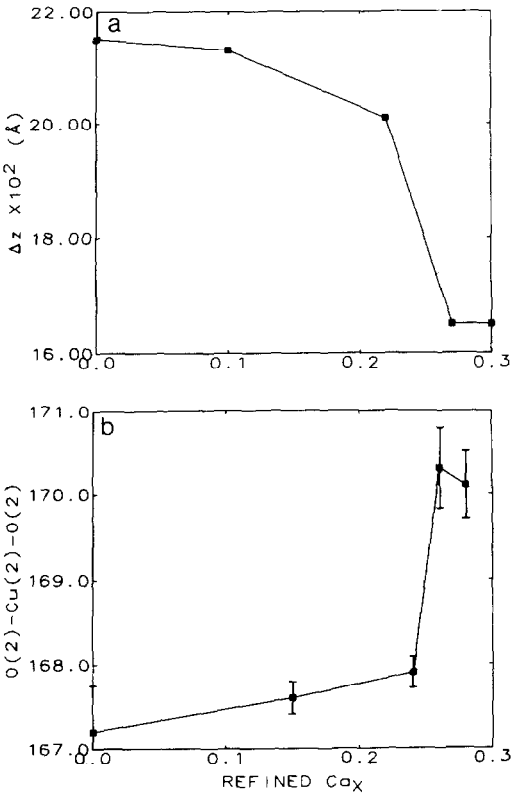

FIG. 6. Variation of (a) sheet flatness ($\Delta z \times 10^2$ Å) and (b) O(2)–Cu(2)–O(2) angle (equivalent to Cu(2)–O(2)–Cu(2) angle) with the refined value of x.

O(1)]; and those varying in a more complex fashion. In this latter class are distances and angles related to the aspect of the double sheet (Fig. 1) such as the O(2)–Cu(2)–O(2) angle (Table III) and intersheet distances (Figs. 4–6).

The presence of a solid solution limit near $x = 0.3$ has been reported (*7*) in the related $(Y_{1-x}Ca_x)Ba_2Cu_3O_{7-\delta}$ system. This also appears to be the case in (Y/Ca)123-O_6. In particular, three observations are consistent with the existence of a solid-solution limit near $x = 0.3$: the *a* cell parameter (Fig. 4, Table II) appears to reach a limit at about $x = 0.3$; the refined value of Ca also reaches a limit close to this value (Table II); and the refined atomic parameters for the Y/Ca phase, in samples with nominal values of $x = 0.4$ and 0.5 (Table II), are equivalent within two estimated standard deviations.

Discussion

1. Structural Variations with Increasing x

The variations in unit cell parameters and interatomic distances and angles (Table III) are consistent with the substitution of Ca(II) for Y(III) causing oxidation only in the Cu sheets (Fig. 1) in $(Y_{1-x}Ca_x)Ba_2Cu_3O_6$. This oxidation (removal of electrons from the $d_{x^2-y^2}$ antibonding orbitals) is reflected in a constant contraction of the in-plane Cu(2)–O(2) distance (Fig. 4b) and a constant elongation of the out-of-plane Cu(2)–O(1) distance (Table III) as *x* increases. Similarly, the *a* unit cell parameter (Table II, Fig. 1a) decreases as *x* increases, consistent with the shortening of the Cu(2)–O(2) bond length. The Cu(1)–O(1) distance, as expected (*1–3*), does not vary within experimental error (Table III). This observation is in agreement with previously reported X-ray absorption measurements (*2*) which indicated a constant amount of Cu(I) in these materials.

On the other hand, the more complex behavior of the *c* cell parameter results from competition between sheet flattening, due to electron removal, and the substitution of the larger Ca(II) for Y(III). At low values of *x*, the distances between atoms across the sheets (Fig. 1) increase as expected for the replacement of the smaller Y(III) by Ca(II) (ionic radius 1.03 and 1.12 Å, respectively; Ref. (*14*)). However, contrasting with the increase found for the O(2)–O(2) distance (Table III), the Cu(2)–Cu(2) and Y/Ca–Cu(2) distances both initially increase and then decrease sharply after $x = 0.15$ (Table II, Fig. 5). In other words, the Cu(2) atoms, facing each other across the sheets, (Fig. 1) come closer together (Table II), while the O(2) atoms move apart. Hence, the individual sheets flatten as *x* increases. Consequently, there is an increase in the O(2)–Cu(2)–O(2) angle and a decrease in the difference (Δ) between the *z*-atomic parameters for Cu(2) and O(2) (Fig. 6). Sheet flattening as Ca replaces Y is observed in other cuprate systems (*15*), some of which also exhibit a similar insulator to superconductor transition ($Tl_2Ba_2(Y_{1+x}Ca_x)Cu_2O_8$, for example).

Moreover, at a critical point (near $x = 0.25$) there is a large change in the aspect of the sheet, as evidenced by sharp decreases in Δz, Cu(2)–Cu(2), and Y/Ca–Cu(2) distances (Table III, Figs. 6a, 5a, and 5b, respectively). It is at roughly this value of *x* that the superconducting fraction for samples synthesized using solid-state techniques is a maximum (*2*) and that the solid-solution limit is reached (*3*). It is tempting to correlate this change in the aspect of the sheet with the onset of bulk superconductivity. However, more work on homogeneous materials is required to test this speculation. We now are carrying out syntheses at lower temperature, in order to determine if the phase separation observed using electron microscopy (*3*) is due to the conditions of synthesis used in this study. It is desirable to associated structural change with

homogeneous solids so as to better define the relationship of T_c to these observed structural changes.

Finally, the solid solution limit near $x = 0.3$ (Fig. 4a) may also be associated with the discontinuity at $x = 0.25$; i.e., the geometry of the sheets might dictate the amount of Ca which can be accommodated. An analysis, similar to the one presented here, of the structure of $(Y_{1-x}Ca_x)Ba_2Cu_3O_{7-\delta}$ (which also is limited to $0 \leq x \sim 0.3$) (*7*) as a function of x may help in determining whether the geometry of the sheets is indeed critical in fixing the solid-solution limit.

2. *Relationship between* $(Y_{1-x}Ca_x)Ba_2Cu_3O_6$ *and* $Pb_2Sr_2(Y_{1-x}Ca_x)Cu_3O_8$

Replacement of Y(III) by Ca(II) in the parent compound $Pb_sSr_2YCu_3O_8$ has recently been reported to lead to superconductivity (*10–12*). Structurally related to $(Y_{1-x}Ca_x)Ba_2Cu_3O_6$[BaYCa], it can be envisioned as an intergrowth of $YBa_2Cu_3O_6$ and PbO, with PbO (square pyramids) inserted between the linearly coordinated Cu(I) sites and the Cu(II)–O sheets in $YBa_2Cu_3O_6$. Recently, a single-crystal structure determination was performed (*11*) on a sample with a refined composition $Pb_2Sr_2(Y_{0.75}Ca_{0.25})Cu_3O_8$[SrYCa] (or written so as to emphasize the structural relationship with the 123-related material $(Y_{0.75}Ca_{0.25})Sr_2Cu_3O_6 \cdot 2PbO$). Further, XANES measurements (*3, 15*) have confirmed that lead is present as Pb(II) and that the amount of Cu(I) does not vary as Ca replaces Y. The level of oxidation in the CuO_2 sheets in this material will then be the same as it is in $(Y_{0.75}Ca_{0.25})Ba_2Cu_3O_6$ (Figs. 4–6).

Many of the structural changes observed in this study of [BaYCa] are mirrored in the [SrYCa] material. For example, changes in Cu(2)–O(2) bond length and Δz when Ca is doped into the parent compounds are similar in both classes; as 0.25 Ca(II) replaces Y(III), Δz decreases by 0.03 Å for [BaYCa] and by 0.05 Å for [SrYCa] while Cu(2)–O(2), as expected (*15*), contrasts by 0.01 Å for both materials. The Cu(2)–Cu(2) interatomic distance (Fig. 1) also decreases, by 0.023 and 0.031 Å for [BaYCa] and [SrYCa], respectively. Despite this similarity in geometry and level of oxidation, [SrYCa] has a value of T_c at least 10 K higher (*1–3, 10–12*) than that for [BaYCa].

3. *The Dependence of* T_c *on Cu(2)–O(2) Bond Strength*

As has been pointed out in several studies (*16–19*), there appears to be a distinct correlation, at least within the one family of materials, between the in-plane Cu–O interatomic distance, the level of oxidation, and T_c. A compendium of much of this data has recently been presented (*16*) in which the superconductors are considered as three families, those based on La, Sr, and Ba. Each family appears to have a different optimum value of Cu–O bond length; T_c, at this optimum, increases in going from La to Sr to Ba. The conclusion drawn is that a different optimum level of oxidation exists for each class of superconductor. Further, T_c increases as bond strength increases toward the optimum.

Generally, this observation is well supported in the comparison between the structures and properties of [BaYCa] and [SrYCa]. The values of T_c (zero resistance) for [SrYCa] and [BaYCa] at Y/Ca = 3 are 55 and 44 K, respectively (*11, 2*). Since the level of oxidation of the sheet is the same, the difference could be due to the difference in bond strength. Contraction of the Cu(2)–O(2) bond in the case of [SrYCa], because of the presence of the smaller Sr rather than Ba in the structure, increases its bond strength toward its optimum value (*15*). This implies that [SrYCa] is closer to its optimum level of bond strength than is [BaYCa]. Further, the separation between the Sr and Ba families at their respective

optimum bond lengths is given by Wangbo *et al.* (*16*) as 0.02 Å. The difference in the Cu(2)–O(2) bond lengths for [BaYCa] and [SrYCa] is 0.023 Å (Table III, Ref. (*11*)). Interestingly, it is about the same (0.018 Å) for $YBa_2Cu_3O_6$ (*7*) compared with $YSr_2Cu_3O_6 \cdot 2PbO$ (*12*). Although these observations may be fortuitous, it appears that by shifting the "Sr curve" of Wangbo *et al.* (*16*) by 0.02 Å, it would overlap that of Ba. This suggests the difference between these two curves is due largely to a difference in the size of the cations Sr^{2+} and Ba^{2+} (*14–16*). Changing the overall bond strength of the Cu–O bond may therefore be complementary to oxidation of the CuO_2 sheets as a means of adjusting T_c in these materials.

Conclusion

Substitution of Ca(II) for Y(III) in $YBa_2Cu_3O_6$ leads to oxidation of the CuO_2 sheet and bulk superconductivity (T_c = 44 K) at about x = 0.25. Structurally this corresponds to a flattening of the [Cu(2)–O(2)] sheet with respect to $YBa_2Cu_3O_6$, a feature it shares with the structurally related materials derived by Ca substitution into $YSr_2Cu_3O_6 \cdot 2PbO$.

Acknowledgments

The authors thank M. Sweeten for sample preparation and Drs. C. C. Toradi, M. K. Crawford, P. L. Gai, and W. E. Farneth for helpful discussions. Thanks also go to Joan Brady and Sharon Wheeler for typing the manuscript.

References

1. McCarron, E. M., III, Crawford, M. K., and Parise, J. B., *J. Solid State Chem.* **78,** 192 (1989).
2. McCarron, E. M., III, Parise, J. B., Crawford, M. K., and Tranquada, J. M., *in* "Proceedings of the Advanced Materials Conference, Denver, 1989," in press.
3. Parise, J. B., Gai, P. L., Crawford, M. K., and McCarron, E. M., III, *in* "High Temperature Superconductors: Relationships between Properties, Structure, and Solid State Chemistry" (J. B. Torrance, M. Thompson, J. M. Tarascon, J. R. Jorgensen and K. Kitazawa, Eds.), Mat. Res. Soc. Proc., Vol. 156, Pittsburgh, PA, 1989, in press.
4. Bednorz, J. G., and Muller, K. A., *Z. Phys. B* **64,** 189 (1986).
5. Cava, R. J., Van Dover, R. B., Batlogg, B., and Rietman, E. A., *Phys. Rev. Lett.* **58,** 408 (1987).
6. Subramanian, M. A., Gopalakrishnan, J., Torardi, C. C., Askew, T. R., Flippen, R. B., Sleight, A. W., Lin, J. J., and Poon, S. J., *Science* **240,** 495 (1988).
7. See, for example, Yokura, Y., Torrance, J. B., Huang, T. C., and Nazzal, A. I., *Phys. Rev. B* **38,** 7156 (1988); Manthiram, A., Lee, S. J., and Goodenough, J. B., *J. Solid State Chem.* **73,** 278 (1988); Jirak, Z., Hejtmanek, J., Pollert, E., Triska, A., and Vasek, P., *Physica C.* **156,** 750 (1988).
8. Farneth, W. E., Bordia, R. K., McCarron, E. M., III, Crawford, M. K., and Flippen, R. B., *Solid State Commun.* **66,** 953 (1988).
9. Cava, R. J., Batlogg, B., Chen, C. H., Rietman, E. A., Zahurak, S. M., and Werder, D., *Nature (London)* **329,** 423 (1987).
10. Cava, R. J., Batlogg, B., Krajewski, J. J., Rupp, L. W., Schneemeyer, L. F., Siegrist, T., Van Dover, R. B., Marsh, P., Peck, W. F., Jr., Gallagher, P. K., Glarum, S. H., Marshall, J. H., Farrow, R. C., Waszczak, J. V., Hull, R., and Trevar, P., *Nature (London)* **336,** 211 (1988).
11. Subramanian, M. A., Gopalakrishnan, J., Torardi, C. C., Gai, P. L., Boyes, E. D., Askew, T. R., Flippen, R. B., Farneth, W. E., and Sleight, A. W., *Physica C* **157,** 124 (1989).
12. Cava, R. J., Marezio, M., Krajewski, J. J., Peck, W. F., Jr., Santoro, A., and Beech, F., *Physica C* **157,** 272 (1989).
13. Larson, A. C., and Von Dreele, R. B., GSAS Manual, Los Alamos National Laboratory Report LAUR 86-748, 1988.
14. Shannon, R. D., *Acta Crystallogr. Sect. A* **32,** 751 (1976).
15. Parise, J. B., and McCarron, E. M., III, in preparation.
16. Wangbo, M. H., Kang, D. B., and Torardi, C. C., *Physica C* **158,** 371 (1989).
17. Parise, J. B., Herron, N., Crawford, M. K., and Gai, P. L., *Physica C* **159,** 255 (1989).
18. Tarascon, J. M., Greene, L. H., McKinnon, W. R., Hull, G. W., and Geballe, T. H., *Science* **235,** 1373 (1987).
19. Torrance, J. B., Tokura, Y., Nazzal, A. I., Bezinge, A., Huang, T. C., and Parkin, S. S. P., *Phys. Rev. Lett.* **61,** 1127 (1988).